J. Fluid Mech. (1994), *vol.* 276, *pp.* 211–232

Theoretical and experimental studies of three-dimensional wavemaking in narrow tanks, including nonlinear phenomena near resonance

By YITAO YAO, MARSHALL P. TULIN AND ALI R. KOLAINI†

Ocean Engineering Laboratory, University of California, Santa Barbara, CA 93106, USA

(Received 1 October 1993 and in revised form 5 April 1994)

In view of several practical ramifications of this problem, computational–analytical techniques for calculating waves induced by heaving arbitrary bodies in narrow tanks have been developed, including nonlinear wave groups produced near tank resonance. These feature computational near-field solutions matched with appropriate far-field solutions. In the linear case, the far field is provided by linear mode superposition. In the nonlinear case, the far field is described by a suitable nonlinear evolution equation of the cubic Schrödinger type. Matching techniques were developed. Calculations were successfully carried out and the results confirm the important effect of tank walls on added mass and damping.

Results of computations have been compared with some data obtained with a conical wavemaker in a narrow tank. Pronounced nonlinear wave groups were obtained near resonance, and these are well reproduced in some detail by the nonlinear theory and computations, without considering any effects of dissipation.

The related problem of resonant wave groups produced by a segmented paddle wavemaker has also been treated by analysis and subject to computation, with good general agreement with past experiments. The technique features matching near- and far-field computations using energy considerations.

1. Introduction

We carried out some years ago our first experimental studies of shaped wavemakers (Kolaini 1989; Tulin & Kolaini 1988); the majority of our observations were for a cone which heaved on the tank centreline. The observed wave patterns change dramatically in the vicinity of the frequency corresponding to the first (symmetrical) natural transverse mode (first cut-off frequency), and we observed striking effects there, including the suppression of the planar mode and the generation of nonlinear groups of sloshing (transverse) waves. Subsequently we have carried out analyses and numerical computations to explain these observations quantitatively.

The present paper is closely related to two areas of work in the literature. The first area concerns analytical studies of wave effects due to oscillations of a truncated cylinder in a tank, utilizing the linear free-surface approximation, see Yeung & Sphaier (1989 *a*, *b*). The second area concerns theoretical and experimental studies of nonlinear wave group formation by a symmetrical wavemaker operating near the first cut-off

† Current address: National Center for Physical Acoustics, University of Mississippi, Collisium Dr., MS 38677, USA.

(Kit, Shemer & Miloh 1987). The first set of authors focused on the prediction of added mass and damping for heave as well as surge, pitch and sway, over a wide range of frequencies, utilizing linear analytical solutions in series form. In their impressive work, they found sharp but finite peaks and sometimes discontinuities in the computed values of their dimensionless coefficients at the successive cut-off frequencies. The second set of authors concentrated on the measurement and prediction of the nonlinear modulated sloshing wave patterns in the tank near the first cut-off frequency; these were produced by a segmented symmetric paddle wavemaker which was operated so as always to produce zero mean paddle displacement and thus avoid the production of planar waves.

The forces on oscillating bodies are the integration of pressures resulting from the near-field motions, while the wave patterns in the body of the tank themselves define the far-field motions. Yeung & Sphaier avoided the problem of connecting the near and far fields by choosing a body, the truncated cylinder, for which they are able to obtain analytical solutions, including both propagating and evanescent modes, satisfying the linear boundary conditions on the wavemaker, the free surface and the tank walls. Kit *et al.* are largely concerned with wave groups in the far field, which they model with an appropriate nonlinear evolution equation. They have attempted to connect this far-field model and the wavemaker itself by linearizing the wavemaker boundary conditions and applying them on the back wall of the tank. The resulting theory was able to produce intermittent wave group behaviour only after the introduction of large damping, empirically determined.

In our own work we have dealt with both the linear regime (Problem I) of Yeung & Sphaier and the nonlinear regime (Problems II and III) of Kit *et al.* For both regimes we distinguish between the near and far fields. In the near field, in the case of heaving bodies, we employ a boundary-element plus multiple-image computational method; for Problem I, linearized boundary conditions were satisfied on the undisturbed body and free surface; in Problem II the exact boundary conditions were satisfied on the real boundaries. In the far field we employ different representations in the two cases. In Problem I, we utilize a series in terms of normal (free wave) modes, omitting only evanescent modes with rapid decay near the wavemaker. In Problem II, which applies near a cut-off frequency, we utilize the free propagating wave mode plus a nonlinear evolution equation which describes the behaviour of the resonant sloshing mode. This equation is determined using a multiple-scale analysis following the technique used by Jones (1984) and Miles (1985) to treat cross-waves; the original derivation of the nonlinear cubic Schrödinger equation for wave problems in ducts goes back to Aranha, Yue & Mei (1982).

In both Problems I and II, the near- and far-field solutions are required to match on a suitable downtank plane across the tank and the solutions are found simultaneously. The method has the advantage that it may be applied to arbitrary bodies.

In Problem I we have made computations for a series of heaving bodies of conical shape with elliptic cross-section; these were for a range of shapes and relative axes: downtank/crosstank $\gtrless 1$. The circular cross-section (true cone) was studied most extensively, as it was the subject of earlier experiments. These calculations were originally suggested to explain the observed disappearance of the planar mode during oscillation of the cone at the first cut-off, and they did succeed in confirming this observation. As we shall see, however, this striking phenomena is not at all general, depending for a given tank on both the cross-section area and shape of the heaving body. For the cone, we have made calculations of added mass and damping up to and near the first cut-off, and found behaviour very similar to that found by Yeung &

Sphaier for the truncated cylinder. In particular, we have found that the sharp peaks in added mass and damping near the first cut-off have a finite value, which we believe to be actual and not a result of numerical difficulties near the resonant singularity.

In Problem II we have made computations for the heaving cone tested by Kolaini (1989). These calculations reproduced the observed phenomena very well, including wave group size, shape, spacing and propagation speed, and the observed amplitude cut-off effect. No dissipation or other empirical adjustments to the theory were required.

In this paper we also deal separately with the specific case of a paddle-driven nonlinear sloshing wave (Kit *et al.*) (Problem III), produced near tank resonance. An appropriate boundary condition near the wavemaker is derived based on an energy balance, and this purely inviscid theory leads to a stronger periodical wave group than measured. When a correction is made for energy dissipation at the wavemaker, good agreement in shape, speed, and amplitude of propagating groups can be obtained with the data of Kit *et al.* (1987).

2. Basic equations

Consider a heaving wavemaker with characteristic lengthscale D, operating at one end of a uniform horizontal channel of breadth b in which the undisturbed depth of liquid is d, the angular frequency of the periodic motion of the wavemaker is ω, a is the stroke of the wavemaker and g is the acceleration due to gravity. The flow is assumed to be incompressible, inviscid and irrotational. Dimensionless variables are defined using a as an amplitude scale, $k^{-1} = g/\omega^2$ as a lengthscale and ω^{-1} as a timescale. Then the exact equations to be satisfied are:

$$\nabla^2 \Phi = 0, \tag{2.1a}$$

$$\left.\begin{aligned} \frac{\partial \Phi}{\partial z} - \frac{\partial \eta}{\partial t} &= \epsilon \frac{\partial \Phi}{\partial x_i}\frac{\partial \eta}{\partial x_i} \\ \frac{\partial \Phi}{\partial t} + \eta &= -\tfrac{1}{2}\epsilon \frac{\partial \Phi}{\partial x_i}\frac{\partial \Phi}{\partial x_i} \end{aligned}\right\} \quad \text{at} \quad z = \epsilon\eta, \tag{2.1b}$$

where $\epsilon = ka$;

$$\frac{\partial \Phi}{\partial y} = 0 \quad \text{at} \quad y = \pm \tfrac{1}{2} bk \quad \text{(sidewalls)}, \tag{2.1c}$$

$$\frac{\partial \Phi}{\partial z} = 0 \quad \text{at} \quad z = -dk \quad \text{(bottom)}, \tag{2.1d}$$

$$\frac{\partial \Phi}{\partial n} = n_z(x, y, z) \sin(t) \quad \text{at} \quad x = f(y, z, \epsilon \sin t) \quad \text{(wavemaker)}, \tag{2.1e}$$

$$\frac{\partial \Phi}{\partial n} = 0 \quad \text{at} \quad x = 0 \quad \text{(backwall)}. \tag{2.1f}$$

We shall consider separately here two problems:

Problem I: linear: ϵ, δ small; frequency domain.

Problem II: Nonlinear: ϵ, δ $(= a/D)$ not small; initial boundary value problem; oscillations started from rest:

$$\Phi(x, y, z; 0) = 0. \tag{2.1g}$$

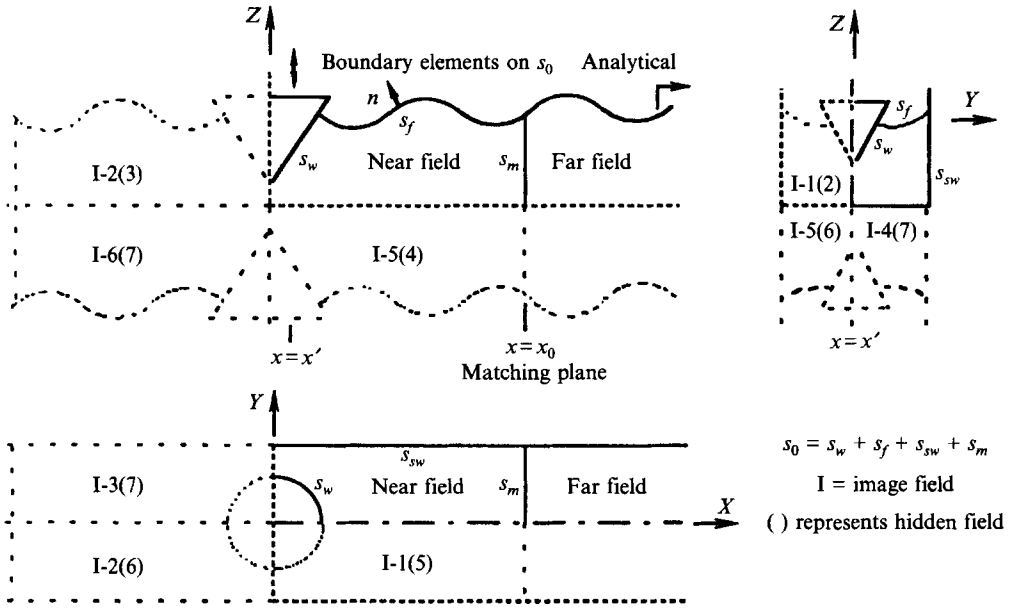

FIGURE 1. Side, front and top views of a large body in a tank showing the division of the fields into near, far and image.

In the case of Problem II, the radiation condition is applied downtank:

$$\Phi(x, y, z, t) \to 0 \quad \text{as} \quad x \to \infty. \tag{2.1h}$$

In the case of the frequency domain calculation (Problem I), it is assumed that the wave energy is flowing downtank only (no reflections considered).

Problem II is especially appropriate in the vicinity of resonant frequencies where the solutions of Problem I become unbounded.

The approach used for both problems is to divide the flow field into a near field (near the wavemaker) and a far field (downtank) where the two separate solutions are matched at an appropriate cross-section ($x = x_0$) (see figure 1), which is chosen to be far enough from the wavemaker that the decaying wave modes generated there may be neglected. The near field is to be determined by the boundary element method, while the far field is to be described in an analytic manner.

Assuming a flow symmetric about the channel centreplane, the field to be computed may be taken as bounded by the centreplane, wavemaker surface, matching plane and the side, bottom, and back walls. The effects of the centreplane, bottom and back walls may be taken into account by use of suitable image systems. There are seven images of the near-field boundary elements, see figure 1.

We note that in the general case of a non-symmetric wavemaker shape, one can use three images of the near-field boundary elements to remove the bottom and back walls.

3. Near field

3.1. *Problem II*

The near field $\Phi(s_0)$ and the velocity normal to s_0, $\Phi_n(s_0)$, are related through Green's third formula:

$$2\pi\Phi(p) + \int_{s_0} \int \left[\Phi(q) \frac{\partial G(p,q)}{\partial n} - G(p,q) \frac{\partial \Phi(q)}{\partial n} \right] \mathrm{d}s = 0, \quad p, q \in s_0, \tag{3.1}$$

where $s_0 = s_w + s_f + s_{sw} + s_m$; $\boldsymbol{n}$ is the normal to the boundary in the outward direction from the fluid domain; $p = x_p$ and $q = x_q$; the Green's function $G(p, q)$ is a simple source $(1/|p-q|)$ plus its seven similar source images.

In (3.1), $\Phi_n(s_{sw})$ and $\Phi_n(s_w)$ are known, (2.1 *c*, *e*). The exact free-surface shape η, and $\Phi(s_f)$ may be determined at each time step through integration of the following relations which apply exactly on s_f:

$$\frac{\mathrm{D}\eta}{\mathrm{D}t} = \frac{\partial \Phi}{\partial z}, \tag{3.2a}$$

$$\frac{\mathrm{D}x}{\mathrm{D}t} = \epsilon \frac{\partial \Phi}{\partial x} \quad \text{and} \quad \frac{\mathrm{D}y}{\mathrm{D}t} = \epsilon \frac{\partial \Phi}{\partial y}, \tag{3.2b}$$

$$\frac{\mathrm{D}\Phi}{\mathrm{D}t} = -\eta + \tfrac{1}{2}\epsilon\left[\left(\frac{\partial \Phi}{\partial x}\right)^2 + \left(\frac{\partial \Phi}{\partial y}\right)^2 + \left(\frac{\partial \Phi}{\partial z}\right)^2\right], \tag{3.2c}$$

where $\nabla\Phi(s_f)$ is known at the previous time step; therefore $\Phi(s_f)$ can be taken as known.

Both $\Phi(s_m)$ and $\Phi(s_m)$ are unknown. They must, however, match their corresponding far-field values on s_m and are therefore related through far-field relationships. These relationships will be discussed subsequently.

3.2. *Problem I*

In this case, ϵ is taken as zero in (2.1); $\Phi = \phi\, \mathrm{e}^{-\mathrm{i}t}$, where ϕ is complex; and the equivalent of (3.1) is

$$2\pi\phi(p) + \int_{s_0}\left[\phi(q)\frac{\partial G(p,q)}{\partial n} - G(p,q)\frac{\partial \phi(q)}{\partial n}\right] \mathrm{d}s = 0, \quad p, q \in s_0, \tag{3.3}$$

where $G(p, q)$ is the same as above.

In the linear case, $\phi(s_f) = \phi_n(s_f)$, where s_f is the undisturbed free surface. As in Problem II, $\phi_n(s_{sw})$ and $\phi_n(s_w)$ are known. On s_m, we will require matching of the near and far field, see §5.

4. Far field

4.1. *Problem I*

The linear far-field free wave modes in the tank are well known, and are represented by three series (in dimensional form):

$$\Phi = \Phi_{\mathrm{I}} + \Phi_{\mathrm{II}} + \Phi_{\mathrm{III}}, \tag{4.1a}$$

where

$$\Phi_{\mathrm{I}} = \sum_{n=0}^{n^*} A_n\, \mathrm{e}^{\mathrm{i}(k_{xn}x - \omega t)} \cos(k_{yn}y) \cosh k_z(z+d), \tag{4.1b}$$

$$\Phi_{\mathrm{II}} = \sum_{n=n^*+1}^{\infty} B_n\, \mathrm{e}^{-k_{xn}x - \mathrm{i}\omega t} \cos(k_{yn}y) \cosh k_z(z+d), \tag{4.1c}$$

$$\Phi_{\mathrm{III}} = \sum_{m=1}^{\infty}\sum_{n=0}^{\infty} C_{mn}\, \mathrm{e}^{-k_{xmn}x - \mathrm{i}\omega t} \cos(k_{yn}y) \cos k_{zm}(z+d), \tag{4.1d}$$

where

$$k_{yn} = n\pi/b, \tag{4.2a}$$

$$\mathrm{I}: \quad k_{xn}^2 = k_z^2 - k_{yn}^2 \geqslant 0 \quad (n \leqslant n^*), \tag{4.2b}$$

$$\mathrm{II}: \quad k_{xn}^2 = k_{yn}^2 - k_z^2 \geqslant 0 \quad (n > n^*), \tag{4.2c}$$

$$\mathrm{III}: \quad k_{xmn}^2 = k_{zm}^2 + k_{yn}^2. \tag{4.2d}$$

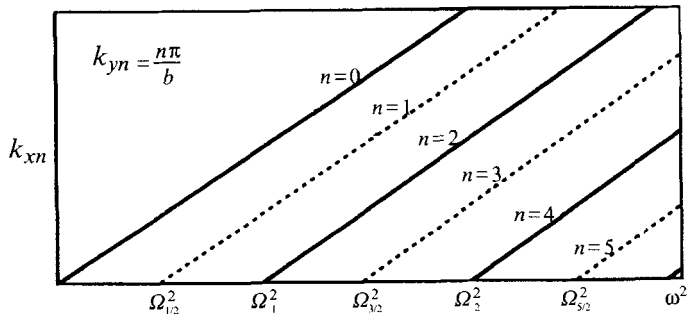

FIGURE 2. Dispersion relation for surface gravity waves in a tank (schematic): ----, asymmetric transverse mode; ——, symmetric mode; $\Omega_{n/2}$, cut-off frequencies.

The wavenumbers, k_z, and k_{zm} in (4.2) are given by the set of dispersion relations

$$\omega^2 = gk_z \tanh(k_z d); \quad \omega^2 = -gk_{zm} \tan(k_{zm} d). \tag{4.3}$$

The first compatibility equation (4.2*b*) reveals that a sequence of propagating wave solutions exists. Each successive solution begins at a cut-off frequency, $\Omega_{n/2}$, for which k_z (given by (4.3)) is equal to transverse wavenumbers, k_{yn}, which are multiples of the half-tank wavenumber, $n\pi/b$, see figure 2.

In the solution (4.1) the first term comprises a finite series of propagating modes for transverse wavenumbers up to and including the preceding cut-off wavenumber, the second comprises an infinite series of evanescent modes for transverse wavenumbers larger than the preceding cut-off wavenumber, the third comprises a double infinite series of evanescent modes for all combinations of transverse and vertical wavenumbers. The asterisk in (4.1) denotes the cut-off condition.

In the case where the wavemaker operates just below (subcritical) or above (supercritical) the first (symmetrical) cut-off frequency, $\Omega_1 = (2\pi g/b)^{1/2}$, only two of the wave solutions given by (4.1), are important in the far field, where most of the evanescent waves have died:

$$\omega < \Omega_1: \quad \phi = A\,e^{ix} \cosh(z+kd) + B \exp[-(\lambda' x)^{1/2}] \cos\left(\frac{2\pi}{kb} y\right) \cosh(z+kd); \tag{4.4a}$$

$$\Omega_1 < \omega < \Omega_2: \quad \phi = A\,e^{ix} \cosh(z+kd) + B \exp[i(-\lambda' x)^{1/2}] \cos\left(\frac{2\pi}{kb} y\right) \cosh(z+kd), \tag{4.4b}$$

where

$$\lambda' = \frac{\Omega_1^4 - \omega^4}{\omega^4} = \left(\frac{2\pi}{bk}\right)^2 - 1 \tag{4.5}$$

is a small parameter of the problem, and the complex numbers A and B are to be determined by solving the entire problem coupling the near and far fields.

It is seen that the B-component in (4.4) changes across the cut-off frequency, Ω_1, from a decaying mode (subcritical) to a propagating mode (supercritical). Since only propagating modes are associated with damping, this has the consequence that B contributes to the damping only for supercritical conditions, resulting in a discontinuity in damping across Ω_1. The added mass is associated with modes of Φ out of phase with the stroke, both propagating and decaying.

It is fundamental that energy supplied to a given mode (the damping) will propagate downtank at the group velocity c_g of that mode. As a result, for a given quantity of modal damping, the modal energy density within the far field will vary as $(c_g b)^{-1}$.

It is easily shown that within the framework of linear theory, c_g varies as $(-\lambda')^{1/2}$, and thus disappears at Ω_1. As a result, unbounded energy density normally appears at the cut-off frequency and destroys the validity of the linearized theory. It is interesting to realize that this occurs even in the case of finite damping.

4.2. *Problem II*

Here we consider only tanks sufficiently deep ($d > \frac{1}{2}b$) so that the deep-water approximation suffices near the first cut-off. As discussed in the Introduction, an evolution equation for the intermittent wave groups may be determined by a multiple-scale analysis. Following Jones (1984), the slow variables which correctly scale the wave group phenomena are

$$X = \epsilon x, \quad \tau = \epsilon^2 t. \tag{4.6}$$

The potential and wave elevation are expanded in ϵ:

$$\Phi = \Phi_1 + \epsilon\Phi_2 + \epsilon^2\Phi_3 + O(\epsilon^3), \tag{4.7a}$$

$$\eta = \eta_1 + \epsilon\eta_2 + \epsilon^2\eta_3 + O(\epsilon^3). \tag{4.7b}$$

Multiple-scale analysis produces first- and second-order solutions. The latter are very lengthy in the case where a planar wave coexists near $\Omega_1 (A \neq 0)$. For brevity we give here only the case $A = 0$ for Φ_2 and η_2:

$$\Phi_1 = A\, \mathrm{e}^z\, \mathrm{e}^{\mathrm{i}(x-t)} + \cos(y)\, \mathrm{e}^z [C(X,\tau)\cos(t) + D(X,\tau)\sin(t)], \tag{4.8a}$$

$$\eta_1 = \mathrm{i}A\, \mathrm{e}^z\, \mathrm{e}^{\mathrm{i}(x-t)} + \cos(y)\, \mathrm{e}^z [C(X,\tau)\sin(t) - D(X,\tau)\cos(t)], \tag{4.8b}$$

$$\Phi_2 = \tfrac{1}{4}[2CD\cos(2t) + (D^2 - C^2)\sin(2t)], \tag{4.9a}$$

$$\eta_2 = \cos(2y)\tfrac{1}{4}[(D^2 - C^2)\sin(2t) - 2CD\sin(2t) + (D^2 + C^2)], \tag{4.9b}$$

where C, D are defined in terms of a complex evolution function: $F(X,\tau;\lambda) = C + \mathrm{i}D$. The detuning parameter λ arises naturally, and defines the closeness to the resonant frequency. It is

$$\lambda = \frac{\Omega_1^2 - \omega^2}{\epsilon^2\omega^2} = \frac{(2\pi/bk) - 1}{\epsilon^2}, \tag{4.10}$$

where we note that $\lambda = \lambda'/2\epsilon^2$.

A third-order solvability equation is found in the form of a nonlinear partial differential evolution equation for $F(X,\tau;\lambda)$. We have found

$$\mathrm{i}\frac{\partial F}{\partial \tau} + \frac{1}{4}\frac{\partial^2 F}{\partial X^2} - \tfrac{1}{2}JF + \tfrac{1}{8}|F^2|\,F = 0, \tag{4.11}$$

where

$$J = \lambda + \frac{4\sqrt{(2)} - 5}{14}|A^2|$$

so that in the presence of planar waves J replaces λ as the detuning parameter; it expresses the influence of already existing planar waves of amplitude A upon the generation and propagation of the sloshing wave groups.

5. Matching and numerical details

5.1. *Problem I*

Boundary conditions on s_0 are given, except on s_m where the near and far fields are required to match. For $\omega < \Omega_2$, the far field is represented by only two modes, A and B, see (4.4). The matching is accomplished by requiring $\phi_n^{(\mathrm{near})} = \phi_n^{(\mathrm{far})}$ at each grid

point on s_m and requiring two integrals of ϕ over s_m to match in the near and far fields. These integrals are

$$\int_0^{\frac{1}{2}bk}\int_{-dk}^{0}\phi^{(\text{near})}\cosh(z+kd)\,\mathrm{d}z\,\mathrm{d}y=\int_0^{\frac{1}{2}bk}\int_{-dk}^{0}\phi^{(\text{far})}\cosh(z+kd)\,\mathrm{d}z\,\mathrm{d}y$$
$$=A\,\mathrm{e}^{\mathrm{i}x_0}\tfrac{1}{2}bk\tfrac{1}{4}(\sinh(2dk)+2dk), \tag{5.1a}$$

$$\int_0^{\frac{1}{2}bk}\int_{-dk}^{0}\phi^{(\text{near})}\cos\left(\frac{2\pi}{bk}\right)\cosh(z+kd)\,\mathrm{d}z\,\mathrm{d}y$$
$$=\int_0^{\frac{1}{2}bk}\int_{-dk}^{0}\phi^{(\text{far})}\cos\left(\frac{2\pi}{bk}\right)\cosh(z+kd)\,\mathrm{d}z\,\mathrm{d}y$$
$$=B\exp[\mathrm{i}(-\lambda')^{1/2}x]\tfrac{1}{4}bk\tfrac{1}{4}(\sinh(2dk)+2dk). \tag{5.1b}$$

As a consequence, $\phi^{(\text{near})}=\phi^{(\text{far})}$ on s_m.

The technique described above differs from that used earlier by Yeung (1975), who matched the near- and far-field velocity potentials at each control point in the matching plane and was therefore required to use as many evanescent and propagating modes as the number of matching points. By utilizing the orthogonal conditions between wave modes, the integral matching technique (Yao 1992) used in the present work eliminates that requirement and also ensures the continuity of ϕ across s_m. We prefer the present technique since it eliminates very small pivot elements due to certain evanescent modes and avoids a stiff matrix.

All of the variables in (3.3) and (4.4) are complex, so separation into real and imaginary parts doubles the number of equations. The resulting matrix needs only to be solved separately for each frequency, and was solved by the generalized minimal residual method; approximately 60 seconds CPU time per frequency was required on the IBM 9000. Constant boundary elements were utilized and the control points were taken at the panel centre. Convergence tests were carried out. Approximately 700 panels were utilized on s_0 and convergence within 5% is estimated.

5.2. *Problem II*

The nonlinear evolution equation is discretized by a semi-implicit finite-difference scheme of the Crank–Nicolson type. The nonlinear term is quasi-linearized by the explicit estimation as in Aranha *et al.* (1982). The space step for the far field was chosen as $\Delta X=0.2$, and the time step (Δt) was chosen as one twentieth of the wavemaker period. In order to eliminate the influence of the far end of the tank, the domain of calculation was two to three times as long as the actual one. The solution, F, was taken as zero at the end of the tank. The motion started from rest and F was determined simultaneously with the solution of the near-field problem.

Matching was accomplished by requiring $\Phi_n^{(\text{near})}=\Phi_{1n}^{(\text{far})}$ on s_m and that two integrals of the fields match at s_m. One of these is an integral of Φ over s_m, as in Problem I, and the other an integral of η over the tank width at x_0:

$$\int_0^{\frac{1}{2}bk}\int_{-dk}^{\eta}\Phi^{(\text{near})}\cos(y)\,\mathrm{e}^{z}\,\mathrm{d}z\,\mathrm{d}y=\int_0^{\frac{1}{2}bk}\int_{-dk}^{0}\Phi_1^{(\text{far})}\cos(y)\,\mathrm{e}^{z}\,\mathrm{d}z\,\mathrm{d}y$$
$$=[C(x_0,\tau)\cos(t)+D(x_0,\tau)\sin(t)]\tfrac{1}{8}bk, \tag{5.2a}$$

$$\int_0^{\frac{1}{2}bk}\eta^{(\text{near})}\cos(y)\,\mathrm{d}y=\int_0^{\frac{1}{2}bk}\eta_1^{(\text{far})}\cos(y)\,\mathrm{d}y$$
$$=[C(x_0,\tau)\sin(t)-D(x_0,\tau)\cos(t)]\tfrac{1}{4}bk. \tag{5.2b}$$

These integrals allow the determination of $C(x_0, t)$ and $D(x_0, t)$ through the matrix solution at each time step. We note that there is a truncation error of order (ηk) involved in (5.2*a*).

Since the sloshing wave forms near the wavemaker and has a slow variation downtank, the number of panels in the near field is reduced to approximately two thirds of that in Problem I, and thereby the number of near-field equations to one third, which makes the computation feasible.

Each complete case shown in figure 7 (about 7000 time steps) involved 10 h CPU time on the IBM 9000; or about 7 s per time step.

6. Paddle-driven resonance

Kit *et al.* (1987), Shemer & Kit (1988) and Shemer, Chamesse & Kit (1989) carried out extensive experimental studies of nonlinear sloshing wave group formation using a four-segment paddle-type wavemaker oscillating in the vicinity of the first (symmetrical) cut-off frequency with the prescribed motion preventing the generation of planar waves.

We treat this problem (Problem III) herein with a different approach than they utilized, first trying to understand the nature of the near field and to determine a proper boundary condition for the far-field sloshing wave.

6.1. *Evolution equation*

An evolution equation, (4.11), has been given earlier, governing the far-field sloshing wave. Although using a different scaling and parameters, (4.11) is fully equivalent to that derived by Aranha *et al.* (1982) and Kit *et al.* (1987) except for the addition here of the effect of co-existing planar waves. This equivalence can be easily shown by dimensionalizing the evolution equations. They then all have the same form,

$$\mathrm{i}\frac{\partial \tilde{F}}{\partial \tilde{t}}+\frac{b(gb)^{1/2}}{8\pi(2\pi)^{1/2}}\frac{\partial^2 \tilde{F}}{\partial \tilde{x}^2}+\frac{\omega^2-\Omega_1^2}{2\Omega_1}\tilde{F}+\frac{(2\pi)^2}{8b^3(2\pi gb)^{1/2}}|\tilde{F}^2|\,\tilde{F}=0. \tag{6.1}$$

The evolution equation, (4.11), must now be supplemented by appropriate boundary conditions. For the wavemaker in an infinite channel, (4.11) requires the specification of either F, or some derivative of F, or a combination of both, continuously in time. The specification of the appropriate boundary condition is a delicate matter, to be discussed below.

6.2. *Boundary condition*

We now consider a simple example of a paddle wavemaker which will not generate planar waves, and take its displacement, in the x-direction, to be in dimensionless form

$$x = \epsilon f(y, z)\sin t \approx \epsilon \cos Y\, \mathrm{e}^{z}\sin t. \tag{6.2}$$

The linear solution of this problem, which is given in the Appendix, is instructive. In that solution, the boundary condition in terms of downtank velocity on the rear wall (wavemaker) has no contribution from the propagating wave, but is satisfied by the decaying wave alone. This latter wave does not, however, contribute to the work done by the wavemaker, since it is in phase with the displacement of the wavemaker. To know the work, it is necessary to know the dynamic pressure, ϕ_t, on the wavemaker. The linear theory shows that the far-field progressive wave begins at a distance from the wavemaker varying as $(2\lambda)^{1/2}\epsilon$; therefore, for λ of order one or less and small ϵ, the pressure in the far field may be directly applied at the wavemaker. In this way, a boundary condition for the far field may be derived from a balance between the work

done by the wavemaker, and the energy propagated into the far field. An alternative is to specify the boundary condition in terms of either the transverse or vertical velocities, which are also continuous through the near and far fields in a linear theory. These two approaches will lead to the same form of the boundary condition for the sloshing wave, i.e. for F. However, the latter is more difficult to formulate quantitatively. So the energy balance approach is used here. Furthermore, the former allows empirical adjustments to be made for dissipation at the wavemaker, which was believed substantial in the paddle experiments.

For the velocity potential near the wavemaker, $\Phi(x, y, z, t)$, in the near-resonant case, we take, $\Phi = \phi_D + \phi$, where ϕ_D represents the decaying wave modes, (4.1), and ϕ is the propagating mode defined by (4.8). The boundary condition at the wavemaker can be written as

$$\frac{\partial \Phi}{\partial x} - \epsilon \frac{\partial f}{\partial y}\frac{\partial \Phi}{\partial y} \sin t - \epsilon \frac{\partial f}{\partial z}\frac{\partial \Phi}{\partial z} \sin t = f \cos t \quad \text{at} \quad x = \epsilon f \sin t. \tag{6.3}$$

Further, we make an expansion of (6.3) for small ϵ about $x = 0$ (or $X = 0$). Then, keeping in mind that $\partial\phi/\partial x$ (or $\epsilon\,\partial\phi/\partial X$) has the same order as $\epsilon\,\partial\phi/\partial y$ and $\epsilon\,\partial\phi/\partial z$, the boundary condition at the wavemaker, corresponding to lowest order in ϵ, is

$$\epsilon: \quad \frac{\partial \phi_D}{\partial x} = f \cos t. \tag{6.4}$$

This is consistent with the result of linear theory (see the Appendix): the linearized boundary condition of (6.3) is satisfied by decaying wave modes.

In accordance with the earlier discussion, we apply the hydrodynamic pressure, due to the far-field sloshing wave, directly on the wavemaker surface. The work done by the wavemaker is

$$\begin{aligned} E_i &= \int_0^T \int_0^{2\pi} \int_{-kd}^0 P \Phi_n \, \mathrm{d}z \, \mathrm{d}y \, \mathrm{d}t \approx \int_0^T \int_0^{2\pi} \int_{-kd}^0 -\rho \frac{\partial \Phi}{\partial t}\frac{\partial \Phi}{\partial x} \mathrm{d}z \, \mathrm{d}y \, \mathrm{d}t \\ &= \int_0^T \int_0^{2\pi} \int_{-kd}^0 -\rho D \cos^2(Y)\, \mathrm{e}^{2z} \cos^2(t) \, \mathrm{d}z \, \mathrm{d}y \, \mathrm{d}t, \end{aligned} \tag{6.5}$$

where E_i is the energy extraction within each wavemaker period, P is the linearized dynamic pressure provided by the progressive wave on the wavemaker, approximated by $-\rho\phi_t$, and Φ_n is the normal velocity on the wavemaker, approximated by $\partial\phi_D/\partial x$ (6.4).

It is seen that the work done by the wavemaker depends only upon the far-field potential which is in phase with the wavemaker motion. Consistent with this result, the linear theory finds that the propagating mode evaluated at the wavemaker is in phase with the latter. Therefore, we take here,

$$C(0, \tau) = 0. \tag{6.6}$$

The energy input at the wavemaker propagates as a sloshing wave with the group velocity C_g, and the total outgoing energy per period, E_o, proportional to twice the kinetic energy density at the wavemaker,

$$\begin{aligned} E_o &= 2C_g \int_0^T \int_0^{2\pi} \int_{-kd}^0 \tfrac{1}{2}\rho \left[\left(\frac{\partial \Phi_1}{\partial y} \right)^2 + \left(\frac{\partial \Phi_1}{\partial z} \right)^2 \right] \mathrm{d}z \, \mathrm{d}y \, \mathrm{d}t \\ &= C_g \int_0^T \int_0^{2\pi} \int_{-kd}^0 \rho D^2 \, \mathrm{e}^{2z} \sin^2(t) \, \mathrm{d}z \, \mathrm{d}y \, \mathrm{d}t. \end{aligned} \tag{6.7}$$

Equating E_i to E_o, the boundary condition at the wavemaker becomes

$$F(0,\tau) = -\mathrm{i}\alpha_1 = -\mathrm{i}\frac{1}{2C_g}, \tag{6.8}$$

where C_g is still unknown. So an iteration is needed to solve the problem.

Shemer & Kit (1988) and Shemer *et al.* (1989) show, in their experiment, that there is high dissipation at the wavemaker since there are large gaps between the paddles and a pair of angles lying vertically on each paddle, which cause strong separation and vortex shedding even in the case when all segments are operated in phase. The experiment also shows that the removal of the angles from the paddles caused a marked difference in the observed sloshing wave behaviour in the tank, where more rapidly modulated sloshing wave groups were observed. On the basis of this evidence, the numerical prediction, with the inviscid boundary condition (6.8), can be expected to produce a more rapidly modulated periodical sloshing wave group.

In order to reproduce the experiment results, the dissipation near the wavemaker needs to be considered. The energy balance then became,

$$E_o = E_i - E_D = (1-\gamma)E_i, \tag{6.9}$$

where the damping ratio, γ, must be determined experimentally, or, as in this case, numerically to match the experimental data.

Then the boundary condition near the wavemaker (6.8) becomes

$$F(0,\tau) = -\mathrm{i}\alpha_1 = -\mathrm{i}(1-\gamma)\frac{1}{2C_g}. \tag{6.10}$$

The boundary condition (6.8) or (6.10) will ensure a nearly constant value of amplitude and phase of $F(0,t)$ near the wavemaker as observed in the experiment (Kit *et al.* 1987; Shemer *et al.* 1989).

7. Numerical results and comparisons

The heaving experiments (Problems II and I) of Kolaini (1989) and Yao (1992) were carried out in a wave tank of cross-section 3 ft square and length 75 ft with a conical wavemaker of 76° total angle, and with family of conical bodies of elliptical cross-section; the average water depth was 60 cm, the average draught of the conical wavemaker was 23 cm and its diameter was 33.3 cm.

7.1. *Problem I*

The amplitude of the propagating planar wave in the case of the conical body was observed to disappear at Ω_1 during the tests. In figure 3, the results of linear calculations confirm a very small value of the wave amplitude there (about 0.5% of the stroke). However, in the case of the widest tank calculated ($b/D = 6.0$), the wave amplitude at Ω_1 is only slightly smaller than its maximum value.

The behaviour of the planar wave amplitude approaching Ω_1 was found to depend upon the body shape. The results of calculations for conical bodies of constant total volume but of various elliptical cross-sections are shown in figure 4; note that the depth in this case was increased over that in figure 3, in order to accentuate the effects. These reveal that elongation of the body along the wavemaker alleviates the tendency for the wave to disappear, whereas its elongation downtank accelerates its disappearance. These results show, too, that the observation of disappearance at the cut-off frequency for the cone wavemaker was fortuitous.

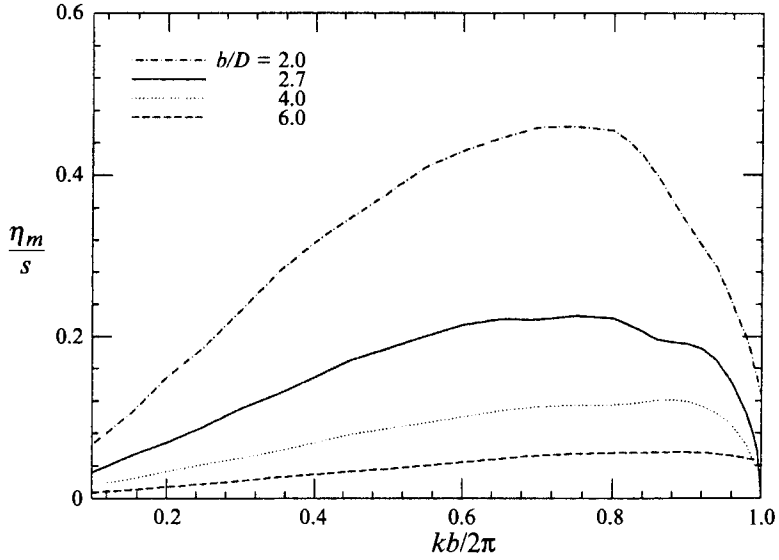

FIGURE 3. Non-dimensional amplitude of the planar wave versus frequency for a half cone wavemaker with various tank widths. $D = 0.33$ m, $h = 0.21$ m.

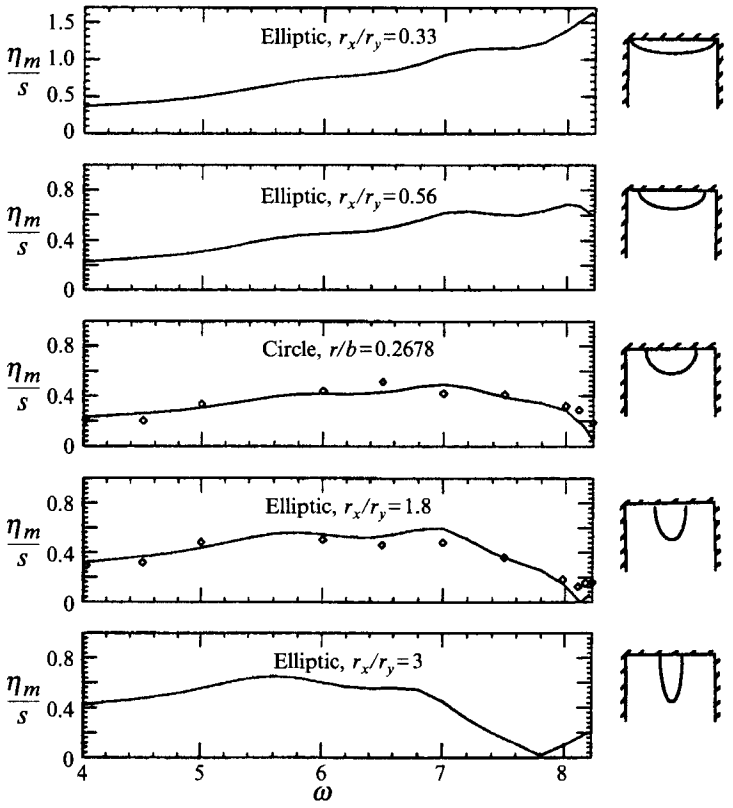

FIGURE 4. Non-dimensional amplitude of the planar wave versus frequency for various wavemakers with constant total volume. (Cut-off frequency $\Omega_1 = 8.233$; $h/b = 0.346$; tank width $b = 0.91$ m.) Symbols are tank experimental data.

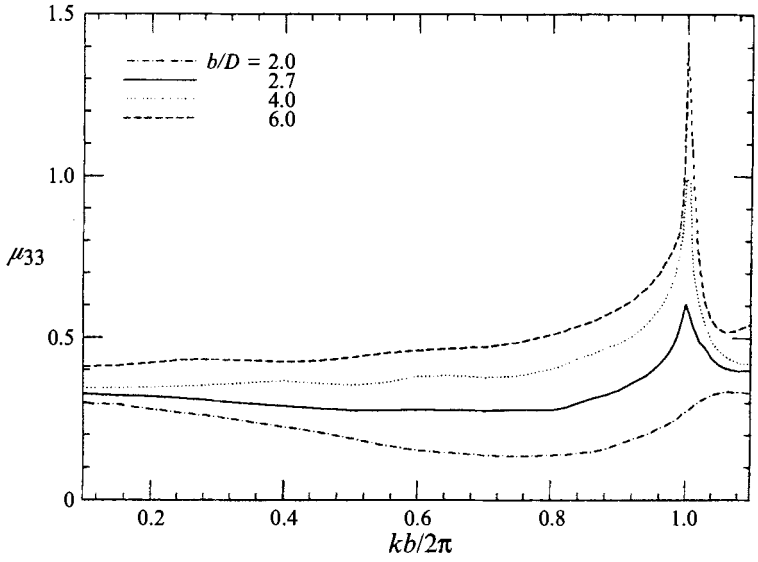

FIGURE 5. Non-dimensional added mass coefficient as a function of $kb/2\pi$ for a half-cone wavemaker with various tanks widths. $D = 0.33$ m, $h = 0.21$ m.

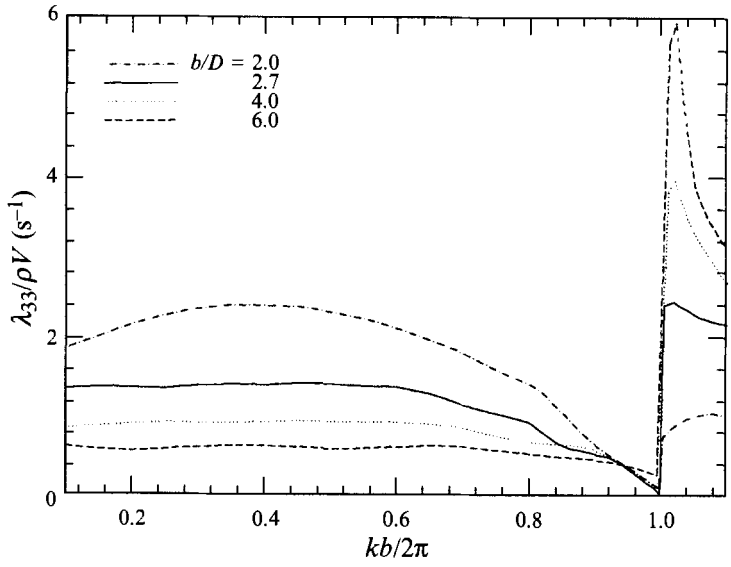

FIGURE 6. Damping factor as a function of $kb/2\pi$ for a half-cone wavemaker with various tank widths. $D = 0.33$ m, $h = 0.21$ m.

If the force on the oscillating body is $F = F_I \sin \omega t + F_R \cos \omega t$, then the added mass coefficient, μ_{33} is equal to $F_R/\rho V a\omega^2$, where V is the body volume. The force was calculated by appropriate integration of the body pressures, $\rho\Phi_t$. The results are shown in figure 5. All of the wave modes, both propagating and evanescent, contribute to the added mass, but the rapid rise to a peak at Ω_1 is due to the contribution of the B-mode which also peaks there; we estimate that about 60–70% of μ_{33} at Ω_1 is due to the B-mode, decaying rapidly on either side of Ω_1. It is interesting that the tank width has a very profound influence on the added mass, everything else being constant. This was already computed and noted by Yeung & Sphaier. They have also shown as we show

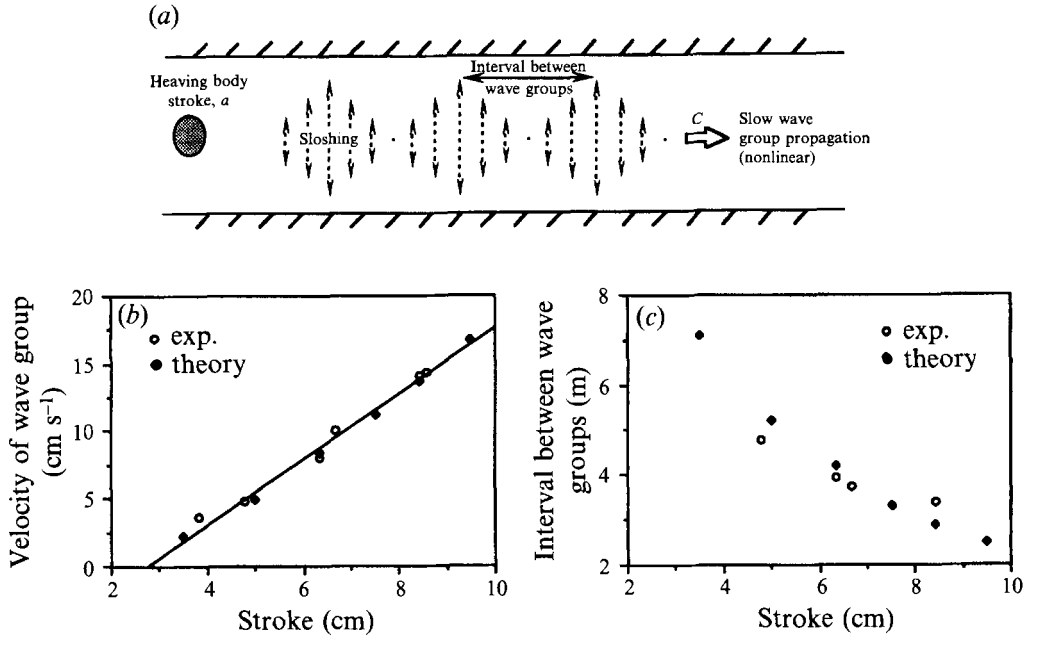

FIGURE 7. Nonlinear sloshing wave group propagation in the channel with various wavemaker strokes at frequency 1.299 Hz (cut-off frequency $f_1 = 1.308$ Hz). (*a*) The situation near tank resonance; (*b*) group speed; (*c*) group interval.

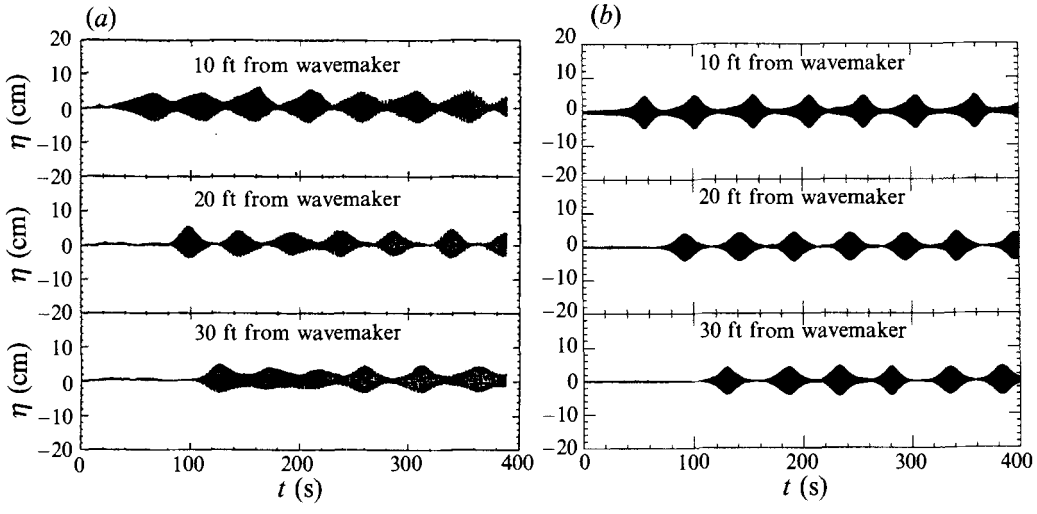

FIGURE 8. Sloshing wave heights as a function of time at various locations along the channel with a wavenumber stroke of 6.35 cm at frequency 1.299 Hz (cut-off frequency $f_1 = 1.308$ Hz). (*a*) Experiment; (*b*) theory.

in figure 5 that narrowing the tank decreases the sharpness of the *B*-peak, and for very narrow tanks causes the peak entirely to disappear.

The damping factor, $\lambda_{33} = F_I/a\omega$, is shown in figure 6 for the cone. The damping decay approaching Ω_1 is due to the suppression of the planar wave, previously noted. The discontinuity across Ω_1 is due to the propagation of the *B*-wave beyond Ω_1 and not below it. Again, the effect on damping near Ω_1 is exaggerated in the case of wider tanks.

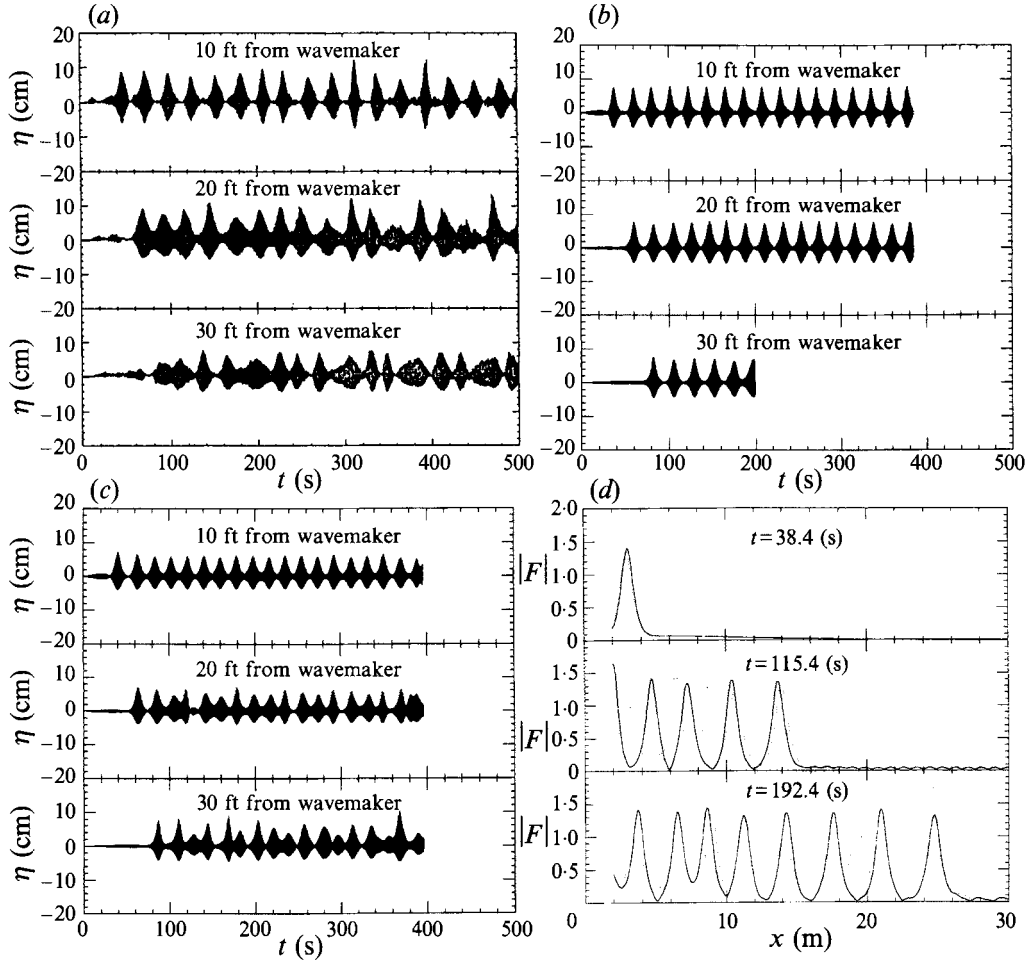

FIGURE 9. Sloshing wave heights as a function of time at various locations along the channel with a wavenumber stroke of 8.41 cm at frequency 1.299 Hz (cut-off frequency $f_1 = 1.308$ Hz). (*a*) Experiment; (*b*) theory (constant width); (*c*) theory (wavy width); (*d*) numerical solution for space-time evolution of $|F|$: ——, with constant tank width; · · · · ·, with variation of width.

7.2. *Problem II*

Kolaini (1989) showed that the heaving motion of the conical wavemaker ($b/D = 2.7$; $d/b = 0.23$) near Ω_1 generally resulted in the continuous intermittent propagation of sloshing wave groups downtank, see figure 7(*a*). Our major result here is to show that these experimental results are closely reproduced by the present theory, which contains no disposable parameters.

An interesting phenomenon first noted by Kolaini is the suppression of the wave group propagation for strokes below a certain value and the linear increase of wave group speed with stroke above this value, see figure 7(*b*). The present theory reproduces the experimental results well. The same is true of the amplitude, spacing, and shape of the groups, see figure 8(*b*).

With increasing stroke, Kolaini found that some of the wave groups become increasingly deformed in shape with increasing distance downtank. Utilizing the present nonlinear theory we have tested the hypothesis that these deformations might

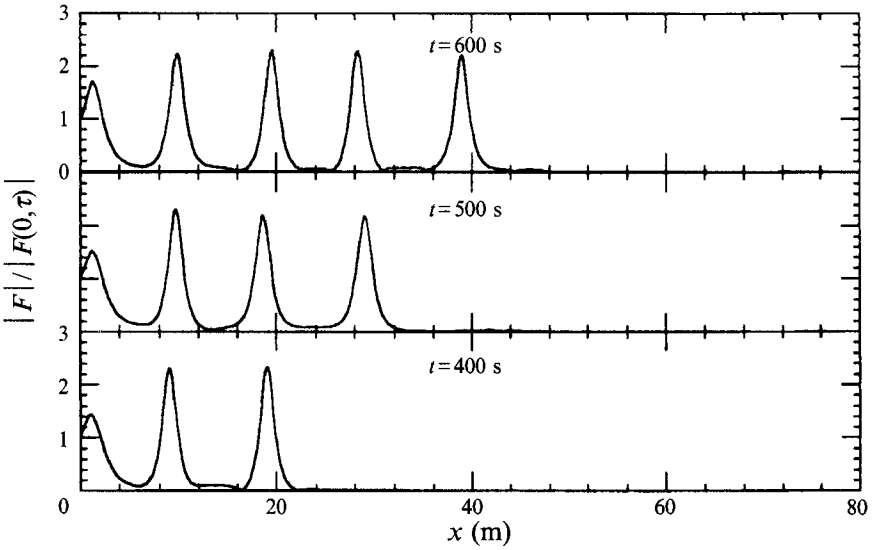

FIGURE 10. Space–time evolution of $|F|/|F(0,\tau)|$ for the case of $|F(0,\tau)| = 7.62$.

be the result of small variations in tank effective width. The results of a simulation of the effect of width variations of 0.5% with a period of 4.4 tank widths is shown in figure 9(*c*). The resulting wave group shape deformations are suggestive of those actually measured, see figure 9(*a*), and are certainly highly noticeable when compared to the case of uniform width, see figure 9(*b*). These results suggest the importance of tank precision in such experiments.

The calculated results for large strokes, figure 9(*b*), also reproduce the vertical asymmetry of the measured wave group; this is a consequence of including the second-order solution.

7.3. *Problem III*

Numerical calculations have been made for the same case as the experiment carried out by Kit *et al.* (1987) in a wave tank of 1.2 m wide and 0.6 m in water depth, where the wavemaker operated with the stroke (s) 0.49 cm at frequency 1.13736 Hz which is below the cut-off frequency (1.13795 Hz). The space step in the calculation was chosen as $\Delta x = 0.1$ m, and the time step (Δt) was 0.5 s. In order to eliminate the influence of the far end of tank, the domain of calculation was substantially longer than in actuality. In our computation, the forced boundary condition was increased smoothly to its value, which removed small high-frequency oscillations in the solution.

Using the boundary condition (6.8), the numerical iteration gives $\alpha_1 \approx 7.62$, and produces the periodical wave groups (figure 10) with higher wave amplitude and a faster travel speed than the experimental result, as expected.

Figure 11 shows the space–time evolution of the amplitude of the sloshing wave from the numerical calculation, for $\gamma = 0.76$, where boundary condition (6.10) has been used and numerical iteration gives $\alpha_1 \approx 3.55$. The direct comparison (figures 12 and 13) between numerical and experimental results gives reasonable agreement in the velocity (4.5 cm s^{-1} numerically and 4 cm s^{-1} experimentally) and periodicity (475 s numerically and 490 s experimentally) of the sloshing wave group. The amplitudes of the soliton also agree well between numerical and experimental results.

There is a discrepancy between the numerical result and experimental observation in the space variation of the soliton shape. Although they show very much the same

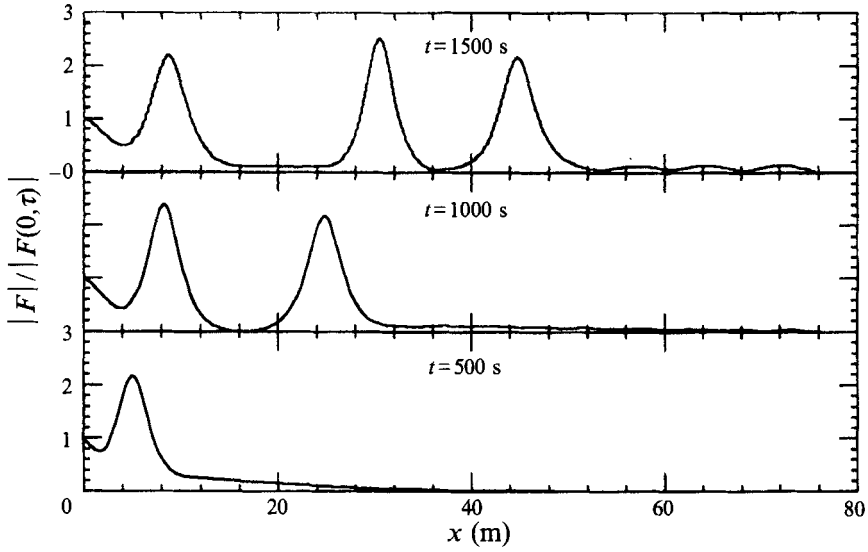

FIGURE 11. Space–time evolution of $|F|/|F(0,\tau)|$ for the case of $|F(0,\tau)| = 3.55$.

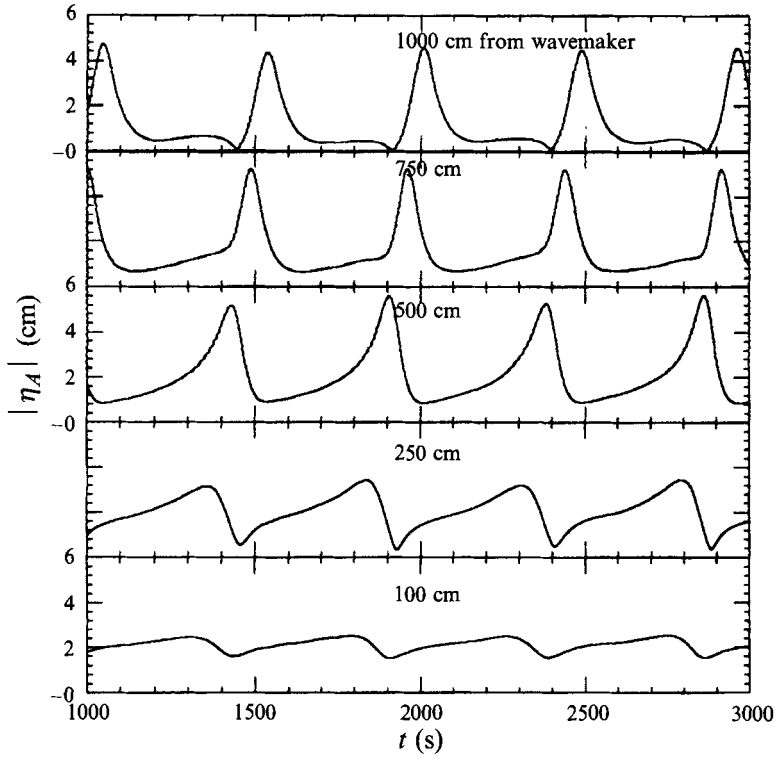

FIGURE 12. Sloshing wave heights as a function of time at various locations along the channel – numerical solution.

tendency and similar forms, the variation is more rapid in the experiment than in the numerical calculation, presumably due to incomplete modelling of the strong dissipative processes which occur at the wavemaker.

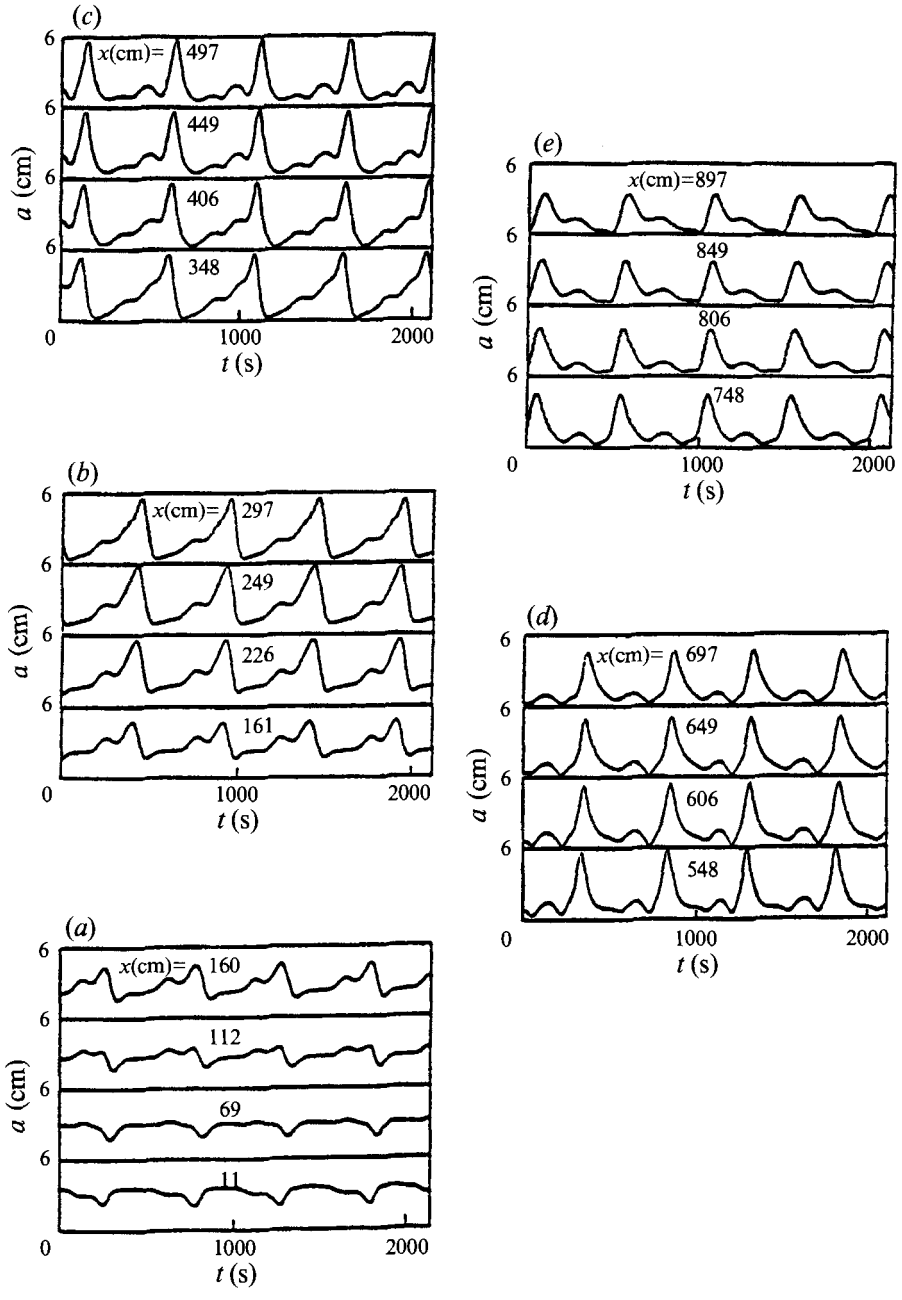

FIGURE 13. Sloshing wave heights as a function of time at various locations along the channel – experimental results (Kit *et al.* 1987).

8. Discussion and summary

The detailed success of the computations presented here in the case of heaving bodies demonstrates the utility of near–far field matching to deal with problems of wave generation in tanks by large and rather arbitrarily shaped bodies. The present paper shows, furthermore, how to carry out the matching.

The results obtained in the linear case confirm many of the findings of Yeung & Sphaier (1989*a*, *b*) concerning the strong effect of tank walls on the added mass and damping of oscillating bodies. Our own interest in the linear calculation of the planar propagating wave was motivated by the experimental finding of Kolaini (1989) that this wave disappeared at the first symmetric cut-off frequency in the case of a cone of 76° total angle with a diameter/tank width ratio about 0.36. This striking observation was confirmed by the linear computations. But they also revealed that disappearance could occur at subcritical frequencies for bodies elongated in the downtank direction. There is clearly more to learn about these phenomena in tanks, and it would seem important to do so for the proper interpretation of wave-induced forces on bodies in tanks.

When oscillating a body near the first symmetric resonance, large sloshing waves can be generated near the body, which intermittently leave it to propagate downtank as a wave group. These had previously been observed and studied by Kit *et al.* (1987). Kolaini (1989) has measured these wave groups and found that they were generated only for sufficiently large heaving strokes, and that they propagated with speeds increasing linearly with further increase in stroke. The theoretical prediction of these properties has not been possible based on previously existing theory. It was for this reason that we instituted the near–far field approach, involving a boundary element computation in the near field based on nonlinear boundary conditions on the body and the free surface. This approach seems to have succeeded, as not only do the calculations result in propagating wave groups without the introduction of viscous dissipation, but the qualitative behaviour of these groups is reproduced surprising well. This sets the stage for the computational studies of such wave groups. It needs to be mentioned, however, that since the computation for a complete run (7000 time steps) requires 10 h CPU time on an IBM 9000, so the wave tank seems an equally efficient research tool.

For a wavemaker with relatively simple geometry, such as a segmented flap wavemaker which has small displacement around the back wall ($x = 0$), a proper boundary condition for sloshing wave can be found through energy balance. Reasonable agreement has been shown between measurements and predictions.

We would like to further point out that the boundary condition, (9.8) or (9.10), arises through direct forcing of the sloshing wave by the wavemaker. This boundary condition is equivalent to the specification of the boundary condition as $\partial\phi/\partial z = f(y, z, t)$ or $\partial\phi/\partial y = f(y, z, t)$. If a segmented moving bottom (wavemaker) vertically oscillates near the cut-off frequency, the boundary condition for the sloshing wave will also have the same form as (9.8).

Finally we should note that the propagation of directional modes by heaving shaped bodies between tank walls can be used for the generation of directional seas in narrow wave tanks for testing purposes, as suggested originally by Tulin & Kolaini (1988), and that we have utilized specially shaped wavemakers, driven stochastically, in our laboratory.

We wish gratefully to acknowledge that the research reported here was carried out under a research grant with the Ocean Technology Program of the Office of Naval Research, Dr Tom Swean, program manager. We also thank the Computer Center at UCLA for free computation time. And finally, the authors acknowledge useful and important discussions of these problems with both Professor Touvia Miloh of Tel Aviv University and Professor Ronald Yeung of the University of California at Berkeley.

Appendix. Non-planar linear progressive waves generated by a paddle wavemaker

We consider here, in a narrow deep wave tank of breadth b, the generation of linear progressive waves which are driven by a special paddle-type wavemaker with a particular prescribed motion preventing the generation of a planar progressive wave,

$$\tilde{x} = -s \cos k_1 \tilde{y}\, e^{k\tilde{z}} \cos \omega \tilde{t}, \tag{A 1}$$

where $k_1 = 2\pi/b$, and the tilde denotes a dimensional variable. Thus,

$$\frac{\partial \tilde{\Phi}}{\partial \tilde{x}} = \omega s \cos k_1 \tilde{y}\, e^{k\tilde{z}} \sin \omega t = \mathrm{Re}\,\{i\omega s \cos k_1 \tilde{y}\, e^{k\tilde{z}}\, e^{-i\omega \tilde{t}}\}. \tag{A 2}$$

Using a Green's function representation and the method of images, which uses infinite mirror images to eliminate the walls, the velocity potential $\tilde{\Phi} = \mathrm{Re}\,\{\tilde{\phi}\, e^{-i\omega \tilde{t}}\}$ can be represented by the summation of potentials generated by three-dimensional periodic oscillating sources of strength, $\sigma(0, \xi, \eta)\, e^{-i\omega \tilde{t}}$, located at the backwall ($x = 0$), in the range of $-\infty$ to 0 in η and $-\infty$ to $+\infty$ in ξ. The normal velocity of the wavemaker projected on the backwall determines the strength of the sources.

$$\tfrac{1}{2}\sigma(0, \xi, \eta) = \frac{\partial \tilde{\phi}}{\partial n} = -i\omega s \cos k_1 \xi\, e^{k\eta}. \tag{A 3}$$

The spatial velocity potential is given by

$$\tilde{\phi} = \frac{1}{4\pi} \int_{-\infty}^{0} \int_{-\infty}^{+\infty} \sigma(0, \xi, \eta)\, G(\tilde{x}, \tilde{y}, \tilde{z}, 0, \xi, \eta)\, d\xi\, d\eta. \tag{A 4}$$

The Green's function, G, which satisfies the linearized free-surface condition and radiation condition, is

$$G(\tilde{x}, \tilde{y}, \tilde{z}, 0, \xi, \eta) = \frac{1}{r} + \frac{1}{r_1} + 2k\ \mathrm{PV} \int_0^{\infty} \frac{1}{m-k} e^{m(\tilde{z}+\eta)} J_0(mR)\, dm + i2\pi k\, e^{k(\tilde{z}+\eta)} J_0(kR), \tag{A 5}$$

where r and r_1 are the distances from $(\tilde{x}, \tilde{y}, \tilde{z})$ to $(0, \xi, \eta)$ and its image $(0, \xi, -\eta)$, respectively, k is the wavenumber corresponding to the frequency ω, J_0 is a Bessel function:

$$J_0(mR) = \frac{1}{2\pi} \int_{-\pi}^{\pi} e^{imR\cos\theta} d\theta \tag{A 6}$$

where

$$R = [\tilde{x}^2 + (\tilde{y} - \xi)^2]^{1/2}. \tag{A 7}$$

Knowing that only the last term in G, (A 5), can contribute to the progressive wave, we can examine the progressive wave by substituting the last term of G in (A 5) into (A 4). The velocity potential, $\tilde{\phi}'$, for progressive wave is, therefore,

$$\tilde{\phi}' = s\omega k \int_{0\infty}^{-} e^{k\eta}\, e^{k(\tilde{z}+\eta)}\, d\eta \int_{-\infty}^{+\infty} \tfrac{1}{2}(e^{ik_1\xi} + e^{-ik_1\xi})\, J_0[kR(\xi)]\, d\xi. \tag{A 8}$$

Now we only consider the case in which the wavemaker is operating near the cut-off frequency, that is, k is very close to k_1. We assume that kb ($\approx 2\pi$) is sufficiently

large, so that the asymptotic evaluation of the second integral in (A 8) can be found by applying the method of stationary phase; that leads to

$$\tilde{\phi}' \sim \frac{S\omega}{(k^2-k_1^2)^{1/2}} \cos k_1 \tilde{y}\, e^{k\tilde{z}} \exp\left[i(k^2-k_1^2)^{1/2}\tilde{x}\right], \tag{A 9}$$

$$\Phi' \sim \frac{S\omega}{(k^2-k_1^2)^{1/2}} \cos k_1 \tilde{y}\, e^{k\tilde{z}} \cos\left[(k^2-k_1^2)^{1/2}\tilde{x}-\tilde{\omega}t\right]. \tag{A 10}$$

Using the same dimensionless form as in §2 and small parameter λ', (4.5), equation (A 9) becomes

$$\phi' = \frac{1}{(-\lambda')^{1/2}} \cos\left(\frac{2\pi}{bk}y\right) e^z \exp\left[i(-\lambda')^{1/2}x\right] \quad (k > k_1), \tag{A 11a}$$

$$\phi' = \frac{-i}{(\lambda')^{1/2}} \cos\left(\frac{2\pi}{bk}y\right) e^z \exp\left[-(\lambda')^{1/2}x\right] \quad (k < k_1). \tag{A 11b}$$

Adopting the same parameters ϵ and λ, as (2.1) and (4.10),

$$\epsilon = ks; \quad \lambda = \frac{k^2-k_1^2}{2k^2\epsilon^2}; \quad \text{so} \quad \frac{(k^2-k_1^2)^{1/2}}{k} = (2\lambda)^{1/2}\epsilon, \tag{A 12}$$

(A 10) becomes

$$\Phi' = \frac{1}{(2\lambda)^{1/2}\epsilon} \cos(Y)\, e^z \cos\left[(2\lambda)^{1/2}\epsilon x - t\right]. \tag{A 13}$$

The asymptotic evaluation of the integral in (A 8) shows that the velocity potential at $(\tilde{x}, \tilde{y}, \tilde{z})$ has contributions only from sources around $(0, \xi_0, \eta)$, and the effects of all other sources cancel each other, where

$$\xi_0 = \pm\frac{k_1}{(k^2-k_1^2)^{1/2}}\tilde{x} + \tilde{y} = \pm\frac{\tilde{x}}{(2\lambda)^{1/2}\epsilon} + \tilde{y}, \tag{A 14}$$

so that

$$R(\tilde{x}, \tilde{y}, 0, \xi_0) = \frac{\tilde{x}}{(2\lambda)^{1/2}\epsilon}. \tag{A 15}$$

In the derivation, we also made an asymptotic expansion,

$$J_0[kR(\xi_0)] \sim \left(\frac{2}{\pi kR(\xi_0)}\right)^{1/2} e^{i[kR(\xi_0)-\pi/4]} + O\left(\frac{1}{kR(\xi_0)}\right). \tag{A 16}$$

So the asymptotic solution $\tilde{\phi}'$ is the appropriate solution for the progressive wave only when $(kb)[R(\xi_0)/b]$ is large, that is when $[R(\xi_0)/b]$ is of at least $O(1)$, or

$$x_{min} = k\tilde{x}_{min} \sim O[kb(2\lambda)^{1/2}\epsilon] \sim O[2\pi(2\lambda)^{1/2}\epsilon]. \tag{A 17}$$

This shows that the stationary progressive wave will be formed very close, a distance of $O[2[\pi(2\lambda)^{1/2}\epsilon]$, to the wavemaker as the wavemaker frequency approaches the cut-off frequency.

According to (A 8), the downtank velocity in the progressive wave at the wavemaker, $\partial\tilde{\phi}'/\partial\tilde{x}|_{\tilde{x}=0}$, is identically zero, so that the boundary condition for the downtank velocity must be satisfied by the decaying wave in linear theory. On the other hand,

according to (A 11), the downtank velocity of the progressive wave in the outer field ($x \geqslant x_{min}$) is of $O(1)$.

This shows that the downtank velocity in the progressive wave changes by $O(1)$ within a distance of $O[2\pi(2\lambda)^{1/2}\epsilon]$; i.e. a velocity boundary layer exists at the wavemaker within the propagating wave field. The change in the potential itself, across this boundary layer, is, however, of higher order, $\delta\phi'/\phi' \approx O(4\pi\epsilon^2\lambda)$. As a result, the outer field potential and pressure may be applied on the wavemaker, although the downtank velocity may not be.

The transverse velocity on the wavemaker and on the outer field is, according to (A 11), of $O[1/(2\lambda)^{1/2}\epsilon]$, so that it becomes unsuitably large for λ of $O(1)$ or less, since nonlinear terms will exert their influence. For this reason, a nonlinear analysis is necessary.

REFERENCES

ARANHA, J. A., YUE, D. K.-P. & MEI, C. C. 1982 Nonlinear waves near a cut-off frequency in an acoustic duct – a numerical study. *J. Fluid Mech.* **121**, 456–485.

JONES, A. F. 1984 The generation of cross-waves in a long deep channel by parametric resonance. *J. Fluid Mech.* **138**, 53–74.

KIT, E., SHEMER, L. & MILOH, T. 1987 Experimental and theoretical investigation of nonlinear sloshing waves in a rectangular channel. *J. Fluid Mech.* **181**, 265–291.

KOLAINI, A. R. 1989 Nonlinear waves near the cut-off frequency. PhD Dissertation, Chapter 5, University of California, Santa Barbara.

MILES, J. W. 1985 Note on parametrically excited trapped cross-wave. *J. Fluid Mech.* **151**, 391–394.

SHEMER, L., CHAMESSE, M. & KIT, E. 1989 Measurements of the dissipation coefficient at the wavemaker in the process of generation of the resonant standing waves in a tank. *Exp. Fluids* **7**, 506–512.

SHEMER, L. & KIT, E. 1988 Study of the role of the dissipation in evolution of nonlinear sloshing waves in a rectangular channel. *Fluid Dyn. Res.* **217**, 143–165.

TULIN, M. P. & KOLAINI, A. 1988 Steep short-crested waves produced by a simple three dimensional wavemaker. *Proc. 22nd American Towing Tank Conf.*, pp. 203–207. National Academy Press.

YAO, Y. 1992 Theoretical and experimental studies of wavemaking by a large oscillating body in long tanks, including non-linear phenomena near resonance. PhD Dissertation, University of California, Santa Barbara.

YEUNG, R. W. 1975 A hybrid integral-equation method for time-harmonic free-surface flow. In *Proc. 1st Intl Conf. on Numerical Ship Hydrodynamics, Gaithersburg, MD* (ed. J. W. Schot & N. Salvesen), pp. 581–607. David Taylor Model Basin, Washington, DC.

YEUNG, R. W. & SPHAIER, S. H. 1989*a* Wave-interference effects on a truncated cylinder in a channel. *J. Engng Maths* **23**, 95–117.

YEUNG, R. W. & SPHAIER, S. H. 1989*b* Wave-interference effects on a floating body in a towing tank. *PRADs '89, Varna, Bulgaria, Oct. 23–28.* Bulgarian Ship Laboratory, Varna.